

## A two-dimensional uniplanar transmission-line metamaterial with a negative index of refraction

Francis Elek and George V Eleftheriades<sup>1</sup>

The Edward S. Rogers Sr. Department of Electrical and Computer Engineering,  
University of Toronto, 10 King's College Road, Toronto,  
Ontario, M5S 3G4, Canada  
E-mail: [gelefth@waves.utoronto.edu](mailto:gelefth@waves.utoronto.edu)

*New Journal of Physics* 7 (2005) 163

Received 1 April 2005

Published 8 August 2005

Online at <http://www.njp.org/>

doi:10.1088/1367-2630/7/1/163

**Abstract.** A uniplanar transmission-line (TL) network has been loaded with lumped elements (chip or printed), enabling one to achieve a two-dimensional (2D) uniplanar negative-refractive-index (NRI) metamaterial. The metamaterial consists of a 2D array of unit cells, composed of TL sections connected in series and loaded in a specified manner. The unit cell dimensions can be designed to be much smaller than the operating wavelength, enabling one to identify the structure as an effective medium, with a negative index of refraction. This NRI metamaterial supports transverse electric (TE) waves, as opposed to related previous work on NRI-TL media that supported transverse magnetic (TM) waves. The dispersion characteristics are calculated using a simple, fast 2D loaded TL model with periodic (Bloch) boundary conditions. Subsequently the dispersion relation is simplified in the homogeneous limit, thus allowing one to identify effective permittivities and permeabilities, which are shown to be simultaneously negative. Simulations demonstrating the negative refraction of a plane wave on an interface between such a NRI uniplanar metamaterial and a commensurate positive-refractive-index (PRI) metamaterial verify the validity of the proposed concept and theory. A fully printed unit cell is presented at microwave frequencies ( $\sim 10$  GHz) along with a prescription for synthesizing an isotropic 3D transmission line NRI metamaterial based on this unit cell.

<sup>1</sup> Author to whom any correspondence should be addressed.

**Contents**

<b>1. Introduction</b>	<b>2</b>
<b>2. TL dispersion model</b>	<b>4</b>
<b>3. NRI uniplanar grids</b>	<b>9</b>
<b>4. Fully printed implementation at microwave frequencies</b>	<b>12</b>
<b>5. Microwave simulations confirming negative refraction</b>	<b>14</b>
<b>6. Conclusion</b>	<b>16</b>
<b>Appendix</b>	<b>16</b>
<b>References</b>	<b>17</b>

**1. Introduction**

During the past several years, there has been a renewed interest in the theoretical characterization and physical implementation of composite structures with effective material parameters not encountered in naturally occurring media (metamaterials). An example of an earlier implementation of a composite structure with effective material parameters, albeit one with properties that are normally encountered in nature, is that of an artificial dielectric [1, 2]. Such structures are essentially large-scale models of actual bulk media with the atoms replaced by highly conducting elements. At low frequencies, an effective (positive) dielectric constant may be defined for such structures [2], enabling one to design lenses in the centimetre wavelength regime in a manner similar to the optical design of lenses [1].

More recently, the study of composite media has explored the possibility of implementing structures with more exotic properties, and in particular those with simultaneous negative permittivity and negative permeability. The consequences for a medium having simultaneous negative permittivity and permeability were explored in the seminal paper of Veselago [3], who deduced that the propagation of electromagnetic waves in such media would exhibit the phenomena of backward wave (BW) propagation (although this aspect was only implicitly described), reversed (negative) refraction, reversed Doppler shift, and also a reversal of the Cherenkov radiation. These unusual electromagnetic responses lead to the designation of such materials as negative-refractive-index (NRI) metamaterials. The first reported implementation of an NRI metamaterial consisted of an array of metallic wires, combined with an array of splitting resonators (SRR), which produced effective negative permittivity and negative permeability, respectively [4]. In that work, a frequency band exhibiting negative refraction (BWs) was observed at microwave frequencies.

Another class of NRI media, based on loaded two-dimensional (2D) transmission-line (TL) networks was used to demonstrate negative refraction and focusing. A unit cell for this type of NRI metamaterial consists of sections of microstrip TLs loaded with lumped series capacitors and shunt inductors, either printed or in chip form [5]–[11], with the underlying TLs being connected in shunt. This network was shown to support a fundamental BW band, and it was within the BW band that simultaneous negative permittivity and permeability were defined. By forming a 2D array of such unit cells and creating an interface with another 2D array of unloaded TLs (which are effective positive-refractive-index (PRI) metamaterials) negative refraction and focusing, including a sub-wavelength one, were demonstrated in [11]. In the above described

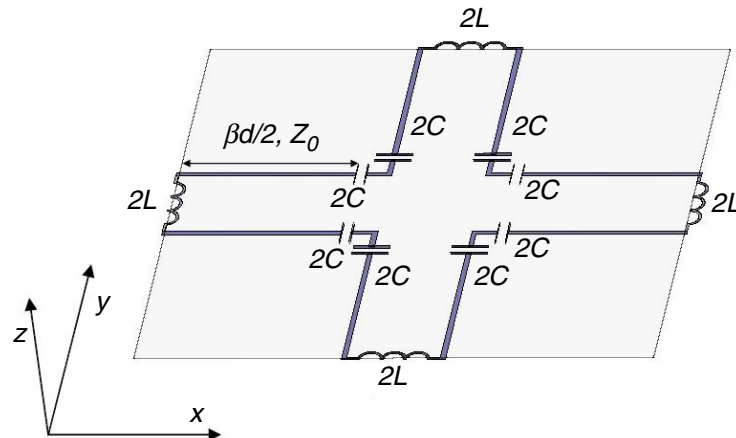


**Figure 1.** 2D equivalent TL circuit of the unit cell for the proposed TE-based structure.

work, the polarization of the waves with respect to the 2D plane defining the NRI metamaterial was transverse magnetic (TM), as the electric field is perpendicular to the plane and the magnetic field is parallel to it.

Interesting alternative structures to the TL-based ones were shown in [12] to exhibit a fundamental BW band as well. That study investigated the dispersion characteristics of 2D arrays of disconnected SRR type of elements printed on a grounded substrate. A nice feature of these designs is that the geometry is uniplanar, and hence they do not require drilled via holes through the substrate. In this paper, we also adopt a uniplanar design, which does not require vias and additionally has no backing ground plane. Although the proposed structure is uniplanar as is that of [12], it is more closely related to the non-resonant structures of [5]–[11] in which loading reactive elements are interconnected with TL sections. An advantage of the TL-based implementation as compared to the use of SRR type of elements is that it does not explicitly rely on resonances to synthesize the negative permeability, thus leading to a wider BW bandwidth.

As in [5]–[11], we consider an underlying grid of TLs, loaded with series capacitors and shunt inductors. By employing TL sections, which may be realized with a coplanar strip (CPS) topology, the polarization of the waves on the TLs is converted to transverse electric (TE). The TL approach applied in [5]–[11] and in this paper, are conceptually related to the TL method (TLM) [13] of modelling electromagnetic waves. In the TLM, a 2D medium may be modelled in either the so-called shunt node or the series node, which correspond to 2D networks of TLs connected in shunt and series, respectively. In the TLM language, the NRI metamaterials of [5]–[11] were realized by loading the 2D shunt node in a dual manner, that is, with series capacitors and shunt inductors, as opposed to the series inductance and shunt capacitance, which characterizes an infinitesimal section of an ideal TL. Accordingly in this paper, we investigate the implications of loading the series node in a dual manner. Specifically, the equivalent circuit of a unit cell for the 2D NRI TL metamaterial investigated is depicted in figure 1. It is seen that the unit cell consists of sections of TLs, which are characterized by their intrinsic propagation constant  $\beta$ , length  $d/2$  and characteristic impedance  $Z_0$ . The TLs are loaded with series capacitors of value  $2C$  and shunt inductors of value  $L$  ( $2L$  in the equivalent circuit as the adjacent unit cell also has a  $2L$  inductor in shunt giving an equivalent inductance of  $L$ ). For the  $x$ -axis directed TL segments, the electric field polarization is primarily along the  $y$ -direction, while for the  $y$ -axis directed TLs,

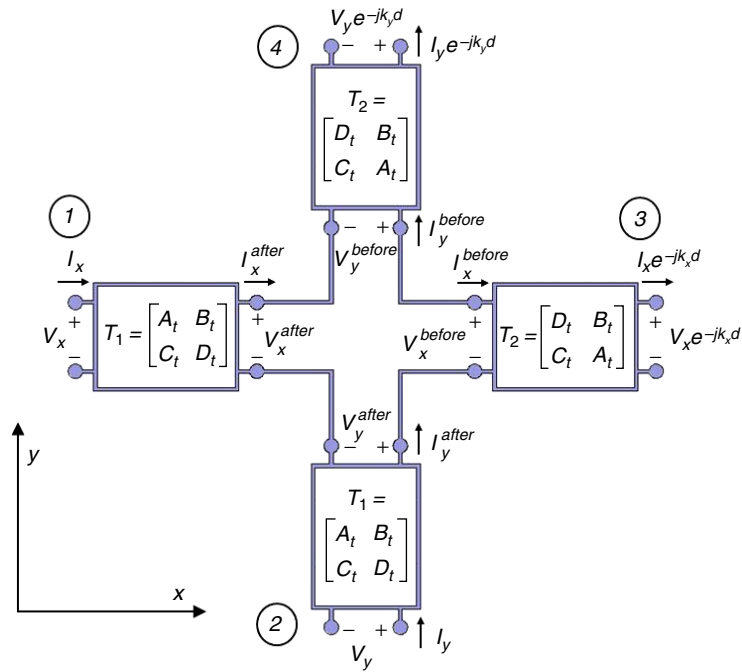


**Figure 2.** Unit cell for a general series connected periodic grid.

the electric field is primarily along the  $x$ -direction. The dominant component of the magnetic field is perpendicular to the plane ( $z$ -axis) for both the  $x$  and  $y$  directed TL segments. Clearly then, relative to the  $x$ - $y$ -plane, the fields are TE polarized as claimed previously. This topology, in addition to having a complimentary polarization (TE rather than TM) with respect to [5]–[11] allows one to simplify the fabrication of a planar NRI metamaterial, as there are no vertically connected components. For example, in the previously described TM-based geometry [5, 6], the microstrip lines are etched on a substrate with a ground plane, with the shunt inductors requiring one to drill holes through the substrate. In the TL geometry described in this paper, both the series loading capacitors and shunt inductors are contained on a single plane, thus obviating the need for drilled via holes.

## 2. TL dispersion model

The unit cell representing the NRI metamaterial (figure 1) is isotropic, as will be the unit cell used to construct the commensurate 2D PRI medium. For such isotropic structures, the propagation characteristics may be simply derived from the network depicted in figure 2. A dispersion analysis along the lines presented in [10] is applied for this purpose. Infinite periodic structures consisting of an array of such unit cells can be analysed by applying the following Bloch (periodic) boundary conditions:

$$V_1 = V_x, \quad V_3 = V_x e^{-jk_x d}, \quad I_1 = I_x, \quad I_3 = I_x e^{-jk_x d}. \quad (1)$$

$$V_2 = V_y, \quad V_4 = V_y e^{-jk_y d}, \quad I_2 = I_y, \quad I_4 = I_y e^{-jk_y d}. \quad (2)$$

This 2D network consists of four 2-port networks connected in series at the central junction. The overall transfer matrix (see appendix) in the transformations  $\{V_x, I_x\} \rightarrow \{V_x^{after}, I_x^{after}\}$  and  $\{V_y, I_y\} \rightarrow \{V_y^{after}, I_y^{after}\}$  has its constituent transfer matrix elements reversed as compared to the transfer matrix for the transformations  $\{V_x^{before}, I_x^{before}\} \rightarrow \{V_x e^{-jk_x d}, I_x e^{-jk_x d}\}$  and  $\{V_y^{before}, I_y^{before}\} \rightarrow \{V_y e^{-jk_y d}, I_y e^{-jk_y d}\}$ . From figure 1, we see that the transformation defined by  $T_1$  of figure 2 is given by  $T_1 = T_{2L} T_{tl} T_C$ , whereas the second transformation matrix,  $T_2$  is given by  $T_2 = T_C T_{tl} T_{2L}$ . It should be noted that  $T_{2L}$ ,  $T_{tl}$  and  $T_C$  represent the transfer matrices for the shunt inductor, the section of TL, and the series capacitor, respectively. Note that the capacitor value for the last matrix is given as  $C$ , this being equivalent to having two  $2C$  capacitors as depicted in the equivalent circuit of figure 1. The effect of reversing the multiplication of the transfer matrices for the two transformations leads to an exchange of the  $A_t$  and  $D_t$  elements of the overall transfer matrices as shown in figure 2. Applying Kirchhoff's current law to the central series connection of the network leads to the following three equations:

$$I_x^{after} = I_x^{before}, \quad I_y^{after} = I_y^{before} \quad \text{and} \quad I_x^{before} = -I_y^{before}. \quad (3)$$

A fourth equation is obtained by applying Kirchhoff's voltage law around the central series connection

$$V_x^{after} + V_y^{before} - V_x^{before} - V_y^{after} = 0. \quad (4)$$

The quantities in (3) and (4) are shown in figure 2. The four equations from (3) and (4) can be related to the boundary conditions in (1) and (2) through the transfer matrices given in figure 2. When these substitutions are made, the following system of homogeneous linear equations is obtained:

$$\begin{bmatrix} f_{11} & f_{12} & 0 & 0 \\ 0 & 0 & f_{23} & f_{24} \\ f_{31} & f_{32} & f_{33} & f_{34} \\ f_{41} & f_{42} & f_{43} & f_{44} \end{bmatrix} \begin{bmatrix} V_x \\ I_x \\ V_y \\ I_y \end{bmatrix} = \begin{bmatrix} 0 \\ 0 \\ 0 \\ 0 \end{bmatrix}, \quad (5)$$

where,

$$\begin{aligned} f_{11} &= C_t(1 + e^{-jk_x d}), & f_{12} &= A_t(e^{-jk_x d} - 1), \\ f_{23} &= C_t(1 + e^{-jk_y d}), & f_{24} &= A_t(e^{-jk_y d} - 1), \\ f_{31} &= C_t e^{-jk_x d}, & f_{32} &= A_t e^{-jk_x d}, \\ f_{33} &= C_t e^{-jk_y d}, & f_{34} &= A_t e^{-jk_y d}, \\ f_{41} &= D_t(1 - e^{-jk_x d}), & f_{42} &= -B_t(1 + e^{-jk_x d}), \\ f_{43} &= D_t(e^{-jk_y d} - 1), & f_{44} &= B_t(1 + e^{-jk_y d}). \end{aligned} \quad (6)$$

Substituting the first two rows of (5) into the last two rows leads to a system of two homogenous equations. For non-trivial solutions, the determinant of the system is set to zero leading to the following dispersion equation

$$A_t C_t (2 \cos(k_x d) + 2 \cos(k_y d) - 4(A_t D_t + B_t C_t)) = 0. \quad (7)$$

As the transfer matrix  $T_1$  is reciprocal, its determinant is set equal to unity, so that  $A_t D_t - B_t C_t = 1$ . Upon substituting this into (7) and simplifying, the dispersion equation becomes

$$\sin^2\left(\frac{k_x d}{2}\right) + \sin^2\left(\frac{k_y d}{2}\right) = -2B_t C_t. \quad (8)$$

The above dispersion relation describes the propagation of waves on a grid of the type shown in figure 1. In order to obtain a better understanding of the above dispersion equation, we will specialize to the case, where the above equation describes nearly homogenous characteristics, that is  $(k_x d) \ll 1$  and  $(k_y d) \ll 1$ . Within this regime, the dispersion equation simplifies to

$$(k_x d)^2 + (k_y d)^2 = -2(2B_t)(2C_t). \quad (9)$$

Before examining the implications of this equation for the unit cell in figure 1, we will consider an unloaded (no loading series capacitor  $C$  and shunt inductor  $L$ ) grid. For such an unloaded grid, the transfer matrix is simply

$$\begin{bmatrix} A_t^{\text{unloaded}} & B_t^{\text{unloaded}} \\ C_t^{\text{unloaded}} & D_t^{\text{unloaded}} \end{bmatrix} = \begin{bmatrix} \cos(\beta d/2) & jZ_o \sin(\beta d/2) \\ jY_o \sin(\beta d/2) & \cos(\beta d/2) \end{bmatrix}. \quad (10)$$

The propagation constant  $\beta$  and characteristic impedance  $Z_o$  of the TL are related to the per-unit-length inductance  $L'_{il}$  and per-unit-length capacitance  $C'_{il}$  by the relations

$$\beta = \omega \sqrt{L'_{il} C'_{il}} = \frac{\omega}{v_{\text{phase}}}, \quad Z_o = \sqrt{\frac{L'_{il}}{C'_{il}}} = \frac{1}{Y_o}, \quad (11)$$

where  $v_{\text{phase}} = \frac{1}{\sqrt{L'_{il} C'_{il}}}$ .

In (11),  $v_{\text{phase}}$  is the phase velocity of the TL mode. As we are considering homogeneous propagation, the small argument approximations are also applied to the TL transfer matrices (this is equivalent to assuming that the sections of TL are electromagnetically short)

$$\begin{bmatrix} A_t^{\text{unloaded}} & B_t^{\text{unloaded}} \\ C_t^{\text{unloaded}} & D_t^{\text{unloaded}} \end{bmatrix} \xrightarrow{(\beta d) \ll 1} \begin{bmatrix} 1 & \frac{1}{2}j\omega L'_{il} d \\ \frac{1}{2}j\omega C'_{il} d & 1 \end{bmatrix}. \quad (12)$$

Substituting (12) into the dispersion equation (9) yields

$$(k_x)^2 + (k_y)^2 = \omega^2 2(C'_{il})(L'_{il}). \quad (13)$$

The unloaded grid of TLs can thus be identified as an effective medium with effective permittivity  $\epsilon_{\text{eff}}^{\text{unloaded}}$  and effective permeability  $\mu_{\text{eff}}^{\text{unloaded}}$  through

$$k^2 = (k_x)^2 + (k_y)^2 = \omega^2 \epsilon_{\text{eff}}^{\text{unloaded}} \mu_{\text{eff}}^{\text{unloaded}}, \quad (14)$$

where  $\epsilon_{\text{eff}}^{\text{unloaded}} \mu_{\text{eff}}^{\text{unloaded}} = 2(C'_{il})(L'_{il})$ , with phase velocity in the effective unloaded medium given as

$$v_{\text{phase}}^{\text{unloaded}} = \frac{1}{\sqrt{\epsilon_{\text{eff}}^{\text{unloaded}} \mu_{\text{eff}}^{\text{unloaded}}}} = \frac{1}{\sqrt{2}} v_{\text{phase}}. \quad (15)$$

The unloaded grid thus supports isotropic, homogeneous propagation, with phase velocity slowed down by a factor of  $\sqrt{2}$  relative to the phase velocity of the TLs comprising the grid. We have found a relation between the product of the effective permittivity and effective permeability and the product of the TL capacitance and inductance per-unit-length. In order to complete the picture, we need to relate these expressions to the wave impedance of a horizontally polarized plane wave (TE wave) propagating horizontally along a homogeneous and isotropic medium. Letting  $k_x = k \cos(\phi)$  and  $k_y = k \sin(\phi)$  (where  $\phi$  is the angle the wave vector  $\vec{k}$  makes with the  $x$ -axis), the  $x$  and  $y$  directed wave impedances are

$$Z_x^{hor-pol} = \sqrt{\frac{\mu_{eff}^{unloaded}}{\epsilon_{eff}^{unloaded}}} \cos \phi \quad (16)$$

and

$$Z_y^{hor-pol} = \sqrt{\frac{\mu_{eff}^{unloaded}}{\epsilon_{eff}^{unloaded}}} \sin \phi. \quad (17)$$

We need to relate the impedances (16) and (17) with expressions that are explicitly related to the periodic structure considered. As the structure is periodic, one may define  $x$  and  $y$  directed Bloch impedances, using the first two rows of (5)

$$Z_x = \frac{V_x}{I_x} = -\frac{f_{12}}{f_{11}} = -\frac{A_t(e^{-jk_x d} - 1)}{C_t(1 + e^{-jk_x d})} = \frac{A_t}{C_t} j \tan\left(\frac{k_x d}{2}\right) \quad (18)$$

and

$$Z_y = \frac{V_y}{I_y} = -\frac{f_{24}}{f_{23}} = -\frac{A_t(e^{-jk_y d} - 1)}{C_t(1 + e^{-jk_y d})} = \frac{A_t}{C_t} j \tan\left(\frac{k_y d}{2}\right). \quad (19)$$

The expressions for the Bloch impedance can be approximated as follows (with the conditions  $(k_x d)$ ,  $(k_y d)$ ,  $(\beta d) \ll 1$ )

$$Z_x^{approximate} = \frac{j(k_x d)}{2C_t} \quad (20)$$

and

$$Z_y^{approximate} = \frac{j(k_y d)}{2C_t}. \quad (21)$$

Identifying these approximated Bloch impedance expressions (20) and (21) with the ideal homogeneous expressions (16) and (17) one obtains

$$\begin{aligned} (Z_x^{hor-pol})^2 + (Z_y^{hor-pol})^2 &= (Z_x^{approximate})^2 + (Z_y^{approximate})^2 \\ \Rightarrow \frac{\mu_{eff}^{unloaded}}{\epsilon_{eff}^{unloaded}} &= \frac{j^2}{2^2 C_t^2} ((k_x d)^2 + (k_y d)^2). \end{aligned} \quad (22)$$

Combining (9), (14) and (22) one obtains

$$\left(\mu_{eff}^{unloaded}\right)^2 = \left(\frac{4jB_t}{\omega d}\right)^2 = (2L'_{il})^2 \Rightarrow \mu_{eff}^{unloaded} = 2L'_{il}. \quad (23)$$

Substituting (23) back into (14) yields

$$\varepsilon_{eff}^{unloaded} = \left(\frac{2C_t}{j\omega d}\right) = C'_{il}. \quad (24)$$

As the unloaded TL grid will be used as a PRI medium, we will designate the above two effective medium parameters as follows:

$$\mu_{eff}^{PRI} = \mu_{eff}^{unloaded} = 2L'_{il}, \quad \varepsilon_{eff}^{PRI} = \varepsilon_{eff}^{unloaded} = C'_{il}. \quad (25)$$

From (23), we see that the effective permeability,  $\mu_{eff}^{PRI}$  is related to the  $B_t$  component of the transfer matrix, while from (24) the effective permittivity,  $\varepsilon_{eff}^{PRI}$  is related to the  $C_t$  component of the transfer matrix  $T_1$ . From the transfer matrix for the PRI medium (12), we see that  $B_t$  is related to the per-unit-length inductance of the TL segments, while  $C_t$  is related to the per-unit-length capacitance of the TL segments. By incorporating the Bloch impedance relations with the dispersion equation, we are able to conclude that  $\mu_{eff}^{PRI}$  is twice the per-unit-length inductance,  $L'_{il}$ , while  $\varepsilon_{eff}^{PRI}$  is the per-unit-length capacitance,  $C'_{il}$ , of the TL segments. The increase in  $\mu_{eff}^{PRI}$  relative to the TLs  $L'_{il}$  accounts for the fact that a plane wave travelling on such a grid is slowed down by a factor  $\sqrt{2}$ , relative to waves on the TL segments comprising the grid (15). The above description may be completed by obtaining the relationship between  $V_x$  and  $V_y$ . The first two equations from (5) may be substituted into the third equation yielding the following equation

$$V_x(1 - e^{jk_y d}) = -V_y(1 - e^{jk_x d}). \quad (26)$$

It is interesting to examine the above equation for the case of on-axis (say along the  $x$ -axis) propagation. Under this condition,  $k_y d = 0$ ,  $k_x d \neq 0$  and hence from (26), we see that  $V_y = 0$ . We conclude that on-axis propagation implies that the transverse (to the propagation direction) sections of TL are short circuited at the edge of the unit cell. From standard TL theory, one can show that a short-circuited section of TL of length  $d/2$  has an input impedance given by  $Z_{in} = jZ_o \tan\left(\frac{\beta d}{2}\right)$ . In the electromagnetically short limit the above simplifies to  $Z_{in} = j\sqrt{\frac{L'_{il}}{C'_{il}}}\sqrt{L'_{il}C'_{il}}\omega\frac{d}{2} = j\omega L'_{il}\frac{d}{2}$  with the aid of (11). From this, we infer that the dispersion relation for on-axis propagation is that of a 1D TL loaded periodically with series inductors of value  $L'_{il}d$  (corresponding to twice the input impedance as derived previously, as there are two transverse stubs). In the electromagnetically short limit, it can be easily shown that a (1D) TL loaded periodically with series inductors behaves as an equivalent line with an appropriately increased per-unit-length inductance. In our case, the TL has a per-unit-length inductance of  $L'_{il}$ , and the transverse stubs provide an additional per-unit-length inductance of  $\frac{(L'_{il}d)}{d} = L'_{il}$ . Thus, the per-unit-length inductance of the equivalent circuit for the case of on-axis propagation is doubled, compared to the 1D lines comprising the grid, and becomes  $2L'_{il}$ . This provides us with an alternative way of understanding the factor of 2 in the expression for  $\mu_{eff}^{PRI}$  in (23).

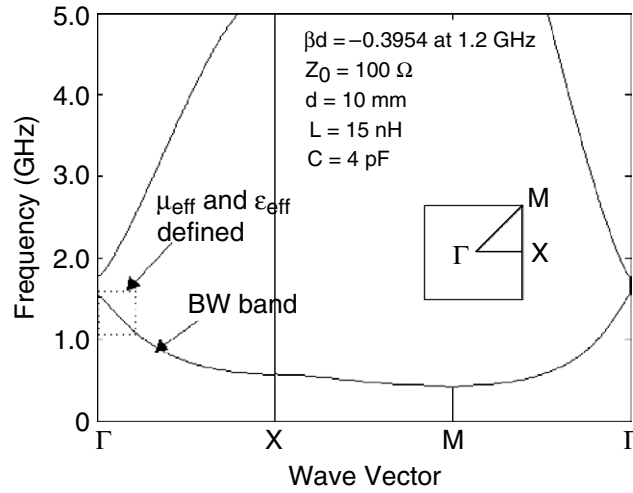


**Figure 3.** Dispersion diagram for the TL-NRI grid used to demonstrate negative refraction.

### 3. NRI uniplanar grids

Upon developing the theory for general isotropic TE-polarization TL grids, we were able to derive dispersion relations and effective material parameters, which were related to the transfer matrix, which defined the grid. We now return to the proposed NRI structure, shown in figure 1. The transfer matrix,  $T_1$  is given by

$$\begin{bmatrix} A_t^{NRI} & B_t^{NRI} \\ C_t^{NRI} & D_t^{NRI} \end{bmatrix} = \begin{bmatrix} \cos\left(\frac{\beta d}{2}\right) & j\left(Z_o \sin\left(\frac{\beta d}{2}\right) - \frac{1}{C\omega} \cos\left(\frac{\beta d}{2}\right)\right) \\ j\left(Y_o \sin\left(\frac{\beta d}{2}\right) - \frac{1}{2\omega L} \cos\left(\frac{\beta d}{2}\right)\right) & \cos\left(\frac{\beta d}{2}\right)\left(1 + \frac{1}{2\omega^2 LC}\right) + \sin\left(\frac{\beta d}{2}\right)\left(\frac{Y_o}{\omega C} + \frac{Z_o}{2\omega L}\right) \end{bmatrix}. \quad (27)$$

Substituting the above into (8), the dispersion relation for the NRI grid becomes

$$\begin{aligned} & \sin^2\left(\frac{k_x d}{2}\right) + \sin^2\left(\frac{k_y d}{2}\right) \\ & = 2\left(Z_o \sin\left(\frac{\beta d}{2}\right) - \frac{1}{C\omega} \cos\left(\frac{\beta d}{2}\right)\right)\left(Y_o \sin\left(\frac{\beta d}{2}\right) - \frac{1}{2\omega L} \cos\left(\frac{\beta d}{2}\right)\right). \end{aligned} \quad (28)$$

The dispersion equation (28), defines the band structure of the TL-NRI grid. The corresponding Brillouin diagram of the NRI grid, which will be used in section 5 to demonstrate negative refraction is shown in figure 3.

At low frequencies, the NRI grid is in cut-off as no propagating mode is supported. As the frequency increases, a BW band emerges at  $k_x d = \pi$ ,  $k_y d = \pi$  ( $M$  point on the Brillouin diagram). Subsequently, above the BW band, another stop-band appears, followed by a FW band. As the structure is periodic, if one were to extend the dispersion to higher frequencies, one would observe a sequence of BW bands followed by FW bands with stop-bands separating them.

The unique feature of the chosen topology is that the lowest band is a BW band, and it is a portion of this band over which negative material parameters may be defined. To observe nearly isotropic, homogeneous propagation, one makes the approximation that the electromagnetic lengths of the interconnecting lines are small,  $\beta d \ll 1$ , and with this approximation  $T_1$  becomes

$$\begin{bmatrix} A_t^{NRI} & B_t^{NRI} \\ C_t^{NRI} & D_t^{NRI} \end{bmatrix} \xrightarrow{\beta d \ll 1} \begin{bmatrix} 1 & j \left( \frac{\omega L'_{il} d}{2} - \frac{1}{\omega C} \right) \\ j \left( \frac{\omega C'_{il} d}{2} - \frac{1}{2\omega L} \right) & \left( 1 + \frac{1}{2\omega^2 LC} \right) + \left( \frac{C'_{il} d}{2C} + \frac{L'_{il} d}{4L} \right) \end{bmatrix}. \quad (29)$$

Additionally, it is required that the phase shifts per-unit-cell are small,  $k_x d \ll 1$ ,  $k_y d \ll 1$ . When these approximations are made, the dispersion equation (28) becomes

$$k^2 = k_x^2 + k_y^2 = \omega^2 2 \left( L'_{il} - \frac{2}{\omega^2 C d} \right) \left( C'_{il} - \frac{1}{\omega^2 L d} \right). \quad (30)$$

Combining the above dispersion equation, with the Bloch impedance formulae, as was done for the PRI medium, one obtains the following formulae for the effective medium parameters:

$$\mu_{eff}^{NRI} = 2 \left( L'_{il} - \frac{2}{\omega^2 C d} \right) \quad (31)$$

and

$$\varepsilon_{eff}^{NRI} = \left( C'_{il} - \frac{1}{\omega^2 L d} \right). \quad (32)$$

It is apparent that the addition of the series loading capacitors,  $2C$ , and the shunt loading inductors,  $L$ , have modified the effective medium parameters from the previous unloaded case. In order to obtain an intuitive understanding of the effective material parameters (31) and (32), one may approximate the equivalent circuit of figure 1 for the case, where the TL segments are short,  $\beta d \ll 1$ . The new approximated equivalent circuit is shown in figure 4.

Each section of TL has been replaced by a series impedance element,  $Z_{il} = j\omega L'_{il} d/2$  cascaded with a shunt admittance element,  $Y_{il} = j\omega C'_{il} d/2$ . The total series impedance for one unit cell (along the  $x$ -axis direction, for example) is

$$Z_{series}^{total} = 2Z_{il} + 4 \left( \frac{1}{j\omega(2C)} \right) = j\omega d \left( L'_{il} - \frac{2}{\omega^2 d C} \right). \quad (33)$$

While, the total shunt admittance for one unit cell is

$$Y_{shunt}^{total} = 2Y_{il} + 2 \left( \frac{1}{j\omega(2L)} \right) = j\omega d \left( C'_{il} - \frac{1}{\omega^2 d L} \right). \quad (34)$$

Thus, the total series impedance  $Z_{series}^{total}$  and the total shunt admittance  $Y_{shunt}^{total}$  are proportional to the effective permeability  $\mu_{eff}^{NRI}$  and the effective permittivity  $\varepsilon_{eff}^{NRI}$ , respectively, with the

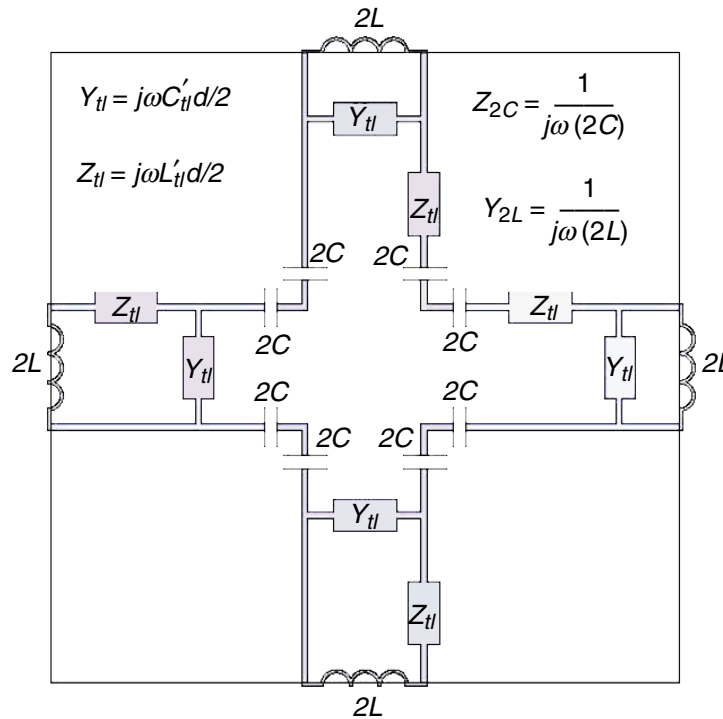


**Figure 4.** Equivalent NRI-TL circuit of the unit cell for the case, where  $\beta d \ll 1$ .

proportionality constant equal to one for  $\varepsilon_{eff}^{NRI}$  and equal to two for  $\mu_{eff}^{NRI}$ . We reiterate once more that the doubling of the effective permeability (31) is obtained, when one combines the dispersion equation with the Bloch impedance expressions.

The expressions (31) and (32) seem to imply that as  $\omega \rightarrow 0$ , both  $\varepsilon_{eff}^{NRI}$  and  $\mu_{eff}^{NRI}$  approach  $-\infty$ . In fact this is not the case, as it is observed that a stop-band exists from 0 Hz up to the onset of the first pass-band at  $k_x d = \pi$ ,  $k_y d = \pi$ . In fact for the lower frequency range of the first pass-band, the conditions of homogeneity,  $(k_x d) \ll 1$  and  $(k_y d) \ll 1$  are not satisfied and hence it is not possible to define meaningful effective parameters. As frequency increases though, one encounters the boxed region in figure 3, where homogenous conditions are satisfied and it is within this region that the effective medium parameters (31) and (32) are both negative. The boxed region is defined by the requirement that  $\varepsilon_{eff}^{NRI}$  and  $\mu_{eff}^{NRI}$  are negative, and simultaneously

$$(kd)^2 = (k_x d)^2 + (k_y d)^2 \ll 1.$$

At this point, we will verify the claim made previously that the region of negative effective parameters is associated with the presence of a BW. Expressing (30) in a slightly modified form

$$k^2 = 2 \left[ \left( L'_tl \omega - \frac{2}{Cd\omega} \right) \left( C'_tl \omega - \frac{1}{Ld\omega} \right) \right] \quad (35)$$

and differentiating both sides of (35), with respect to  $k$  one obtains:

$$2k = 2 \left( L'_{il} \frac{d\omega}{dk} + \frac{2}{Cd\omega^2} \frac{d\omega}{dk} \right) \left( C'_{il}\omega - \frac{1}{\omega Ld} \right) + 2 \left( L'_{il}\omega - \frac{2}{Cd\omega} \right) \left( C'_{il} \frac{d\omega}{dk} + \frac{1}{Ld\omega^2} \frac{d\omega}{dk} \right)$$

$$\Rightarrow k = \omega \frac{d\omega}{dk} \left[ \left( L'_{il} + \frac{2}{Cd\omega^2} \right) (\varepsilon_{eff}^{NRI}) + \left( \frac{\mu_{eff}^{NRI}}{2} \right) \left( C'_{il} + \frac{1}{Ld\omega^2} \right) \right]. \quad (36)$$

Within the region of interest, the quantity in the square brackets is negative, and from figure 3, one sees that the derivative is negative, and hence the right-hand side of (36) is a positive quantity. From this, we conclude that  $k$  and  $d\omega/dk$  are oppositely directed, which is the defining relation of a BW. This confirms that the occurrence of negative effective material parameters coincides with a BW band, as was the case in [5, 6].

The stop-band, which occurs above the BW band may be understood by considering the effective material parameters. Within the BW band, both  $\varepsilon_{eff}^{NRI}$  and  $\mu_{eff}^{NRI}$  are negative, and a propagating BW exists. Within the stop-band, one of the effective parameters changes sign and becomes positive, so that their product is negative and a stop-band is formed. Above the stop-band, both  $\varepsilon_{eff}^{NRI}$  and  $\mu_{eff}^{NRI}$  are positive and a forward wave propagation band is formed. The second stop-band may in fact be closed by setting the frequencies, which correspond to the resonance of  $\varepsilon_{eff}^{NRI}$  and  $\mu_{eff}^{NRI}$  equal to each other

$$\frac{L'}{C'} = 2 \frac{L}{C}. \quad (37)$$

A corresponding 'closure of the stop-band' equation for the TM TL NRI metamaterial was derived in equation (29) of [5].

#### 4. Fully printed implementation at microwave frequencies

As mentioned previously, an advantage of the TE-based implementation explored in this paper, is the ability to make a fully printed planar implementation of the proposed NRI-TL metamaterial. An example of such a printed structure is shown from a top view in figure 5.

The structure is printed on a substrate of permittivity  $\varepsilon_r = 2.3$ , and thickness 3.1 mm, with the other relevant dimensions shown in figure 5. In order to achieve a reasonably large value for the series capacitance, an interdigitated design has been employed. For the printed design, each pair of adjacent  $2C$  capacitors of figure 1 were combined (in series) to give a capacitance of value  $C$ , so that the unit cell of the printed design contains a total of four capacitors of value  $C$ . An equivalent series capacitance of value  $C = 95$  fF has been achieved, as was calculated by performing a scattering analysis for an equivalent geometry. Likewise, as the spacing between the CPS lines will typically be quite small, meandered lines were used to create a reasonable value of shunt inductance. A scattering analysis was also performed for the shunt meandered lines and the equivalent inductance was calculated to be 1.05 nH. The characteristic impedance of the CPS lines is  $163 \Omega$ , while the effective permittivity is  $\varepsilon_{eff} = 1.62$ . The dispersion curve obtained using the loaded TL model (28) is compared with a full wave finite element method (FEM) simulation. The FEM simulation will be performed for the on-axis case, which as mentioned previously is equivalent to an infinite grid, with transverse stubs short-circuited. The results of this simulation are shown in figure 6. The results of the FEM simulation match quite well

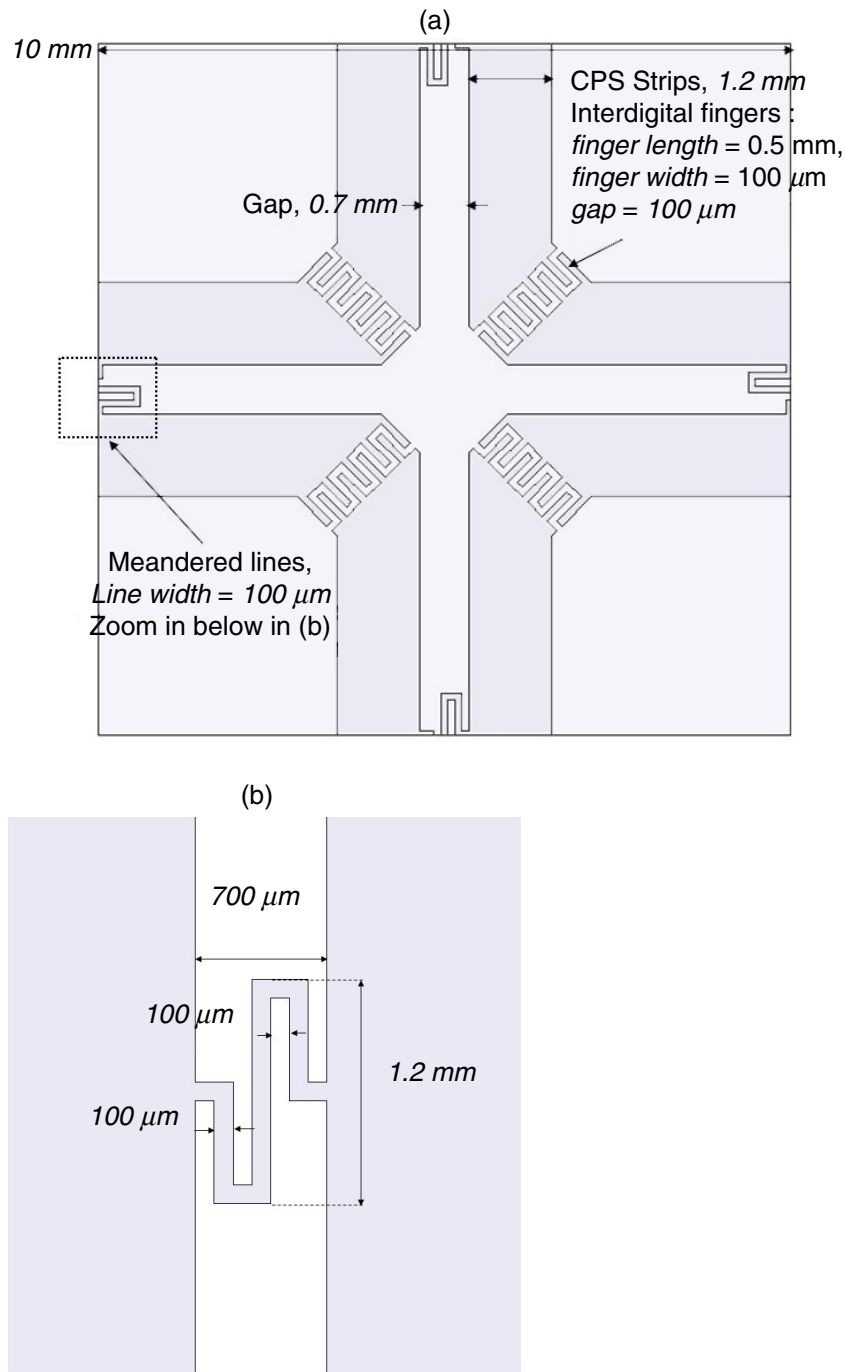


**Figure 5.** (a) Layout for a fully printed design with relevant dimensions; (b) detailed view of the meandered lines.

with the TL-based dispersion curve. Some of the discrepancy between the two curves may be attributed to the approximate nature of the equivalent circuit, as compared with the actual printed implementation. Recalling from figure 1 that in the equivalent circuit model, the lumped components are truly infinitesimal, while the TLs make up the entirety of the actual length of the

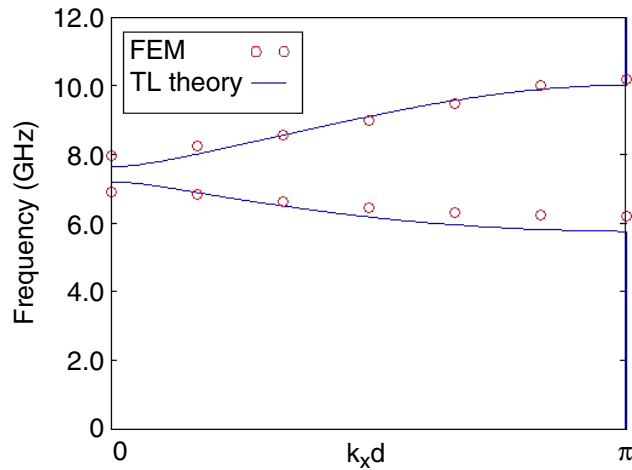


**Figure 6.** On-axis dispersion for the structure of figure 5 comparing FEM simulations with TL theory.

cell. This may be contrasted with the printed design of figure 5, where it is observed that the CPS strips occupy approximately 30% of the width of the unit cell. However, the equivalent circuit model is clearly a valuable tool as it allows one to understand the genesis of the BW band, as well as allowing an excellent first approximation in the design of such metamaterials.

## 5. Microwave simulations confirming negative refraction

In this section, we will use the equations derived previously in order to design a simulation, which confirms the negative refraction of a plane wave incident on the boundary between an NRI-TL metamaterial and a PRI-TL metamaterial.

The NRI-TL metamaterial is chosen as the structure with dispersion relation as shown in figure 3. The NRI metamaterial is defined by the phase delay and characteristic impedance of its underlying TL grid  $\beta_{NRI}d$  and  $Z_o(NRI)$ , respectively, along with the loading series capacitors  $2C$ , and the loading shunt inductors  $L$ . For this implementation, the above quantities are  $\beta_{NRI}d = -0.395$  radians,  $Z_o(NRI) = 100 \Omega$ ,  $C = 4$  pF, and  $L = 15$  nH, at  $f = 1.2$  GHz. For on-axis propagation of the NRI TL metamaterial, one obtains a Bloch impedance,  $Z_x(NRI) = 105.43 \Omega$ , and phase-shift per-unit-cell,  $(k_x d)_{NRI} = 0.499$  radians. We will now proceed to design a PRI TL metamaterial, which has the same on-axis Bloch impedance, and equal but opposite phase shift per-unit-cell. For the PRI grid, the dispersion equation (8) becomes

$$\sin^2\left(\frac{(k_x d)_{PRI}}{2}\right) + \sin^2\left(\frac{(k_y d)_{PRI}}{2}\right) = 2 \sin^2\left(\frac{\beta_{PRI}d}{2}\right). \quad (38)$$

In order to have a wave-vector of equal magnitude in both the NRI and PRI-TL metamaterial, one sets  $(k_x d)_{PRI} = -(k_x d)_{NRI}$ , which gives

$$(\beta_{PRI}d) = -0.3511 \text{ radians}. \quad (39)$$

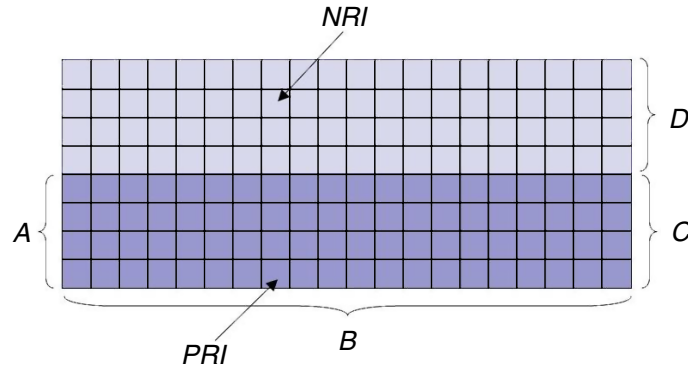


**Figure 7.** Simulation setup for verification of negative refraction.

Using the above value, one may solve for the on-axis Bloch impedance of the PRI-TL using (18), as applied to a PRI-grid

$$Z_x(PRI) = Z_o(PRI) \frac{\tan\left(\frac{(k_x d)_{PRI}}{2}\right)}{\tan\left(\frac{(\beta_{PRI} d)}{2}\right)}. \quad (40)$$

From (40), one can in turn solve for  $Z_o(PRI)$ , with the requirement that  $Z_x(PRI) = Z_x(NRI)$

$$Z_o(PRI) = 73.37 \Omega. \quad (41)$$

With the above, we have designed a PRI-TL metamaterial, which is matched for the case of on-axis propagation, with wave-vectors of equal magnitude and opposite sign. As both the NRI and PRI-TL are nearly isotropic at 1.2 GHz, one may anticipate that the above design will provide a basis for a simulation demonstrating propagation and refraction for the off-axis case.

In order to explore refraction between a PRI and NRI-TL metamaterial, we will use a distributed circuit simulator, which has the capability to implement the real electromagnetic phase delay provided by a section of TL, along with the loading  $L$  and  $C$  lumped components. The grid that will be simulated consists of a PRI-TL of size 20 by 4 unit cells connected to a NRI-TL of size 20 by 4 unit cells, as depicted in figure 7.

A plane wave will be launched from the edge of the PRI grid, by means of voltage sources placed along edges  $A$  and  $B$ . We will consider a plane wave propagating at an angle of  $45^\circ$  to the grid axes, which requires one to phase the sources linearly. For  $k_x d = k_y d$ , one obtains from (38) that  $(k_x d)_{PRI(45^\circ)} = (k_y d)_{PRI(45^\circ)} = -0.3512$  radians =  $-20.12^\circ$ , which is the required source phasing. Additionally from (26), one obtains that  $V_x = -V_y$  for propagation at an angle of  $45^\circ$  to the grid axis. The above results provide one with the proper phasing of sources, and from the Bloch impedance expressions, one finds that the matched termination resistance is  $73.37 \Omega$ , for all of the boundaries. To properly simulate the refraction of an infinite medium, one must also supply a properly phased array of sources along  $D$ . This is necessary, as waves which are incident on  $C$  are absorbed, and hence do not reach the interface, as would occur in a truly infinite medium [10].

The simulated results of the refraction experiment are shown in figure 8. It is observed that the voltage wavefront does indeed refract, with the proper negative angle, upon reaching

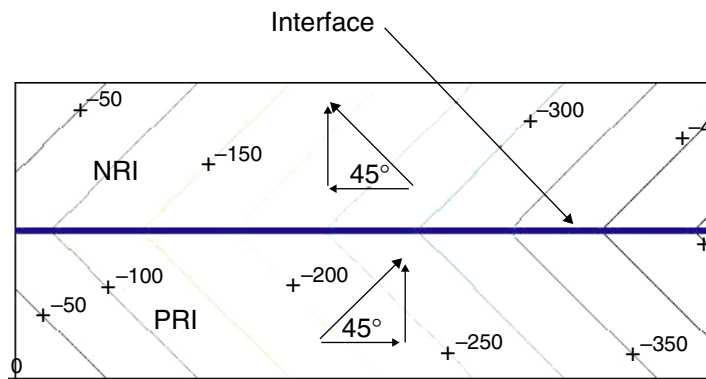


**Figure 8.** Simulated voltage phase contours for negative plane wave refraction.

the interface. Additionally the proper placement of sources along the correct boundaries allows one to observe nearly perfect refraction for a finite structure, in analogy with the TM NRI-TL metamaterials [10].

## 6. Conclusion

In this paper, we have demonstrated a method of implementing a 2D uniplanar NRI-TL metamaterial with no ground plane, and TE-field polarization. An analytical dispersion theory was derived, based on the theory of loaded 2D TL periodic networks. In this way, 2D Brillouin diagrams were generated, clearly demonstrating a fundamental BW band for this structure, which was shown to be the cause of the negative effective permittivity and permeability. The analytical theory provides a comprehensive basis for the design of such metamaterials, as it yields the dispersion characteristics of the structure along with the relevant (Bloch) impedance relations, which are essential for properly matched designs. A fully printed implementation operating in the microwave frequency regime was demonstrated to conform to the derived TL-based theory, exhibiting a BW band of propagation. These results were verified using full-wave FEM simulations. Further simulation results, showing negative refraction of a plane wave incident on a NRI/PRI interface further supported the proposed metamaterial concept and theory developed.

A subtle point that could be made is that the absence of a ground plane in this unit cell opens up the possibility for synthesizing a 3D TL-NRI metamaterial. Specifically, by placing the 2D unit cell of figures on the six faces of a cube one forms a unit cell for a fully isotropic 3D NRI-TL metamaterial. Such a 3D structure has been shown, both analytically, and with full-wave FEM simulations to act as a 3D isotropic NRI metamaterial in [14].

These fully printed uniplanar structures are simple to fabricate and are scalable with frequency from microwave to millimeter-wave/THz frequencies.

## Appendix

The transfer matrix relates the input voltage and current to the output voltage and current, for a given circuit element. Additionally for a cascade of elements, the individual matrices may be

multiplied to arrive at the overall transfer matrix. For example from figures 1 and 2:

$$\begin{bmatrix} V_x \\ I_x \end{bmatrix} = \begin{bmatrix} A_t & B_t \\ C_t & D_t \end{bmatrix} \begin{bmatrix} V_x^{after} \\ I_x^{after} \end{bmatrix}, \quad (\text{A1})$$

where  $T_1 = \begin{bmatrix} A_t & B_t \\ C_t & D_t \end{bmatrix}$  and

$$\begin{bmatrix} V_x^{before} \\ I_x^{before} \end{bmatrix} = \begin{bmatrix} D_t & B_t \\ C_t & A_t \end{bmatrix} \begin{bmatrix} V_x e^{-jk_x d} \\ I_x e^{-jk_x d} \end{bmatrix}, \quad (\text{A2})$$

where  $T_2 = \begin{bmatrix} D_t & B_t \\ C_t & A_t \end{bmatrix}$ .

The matrices  $T_1 = T_{2L} T_C$  and  $T_2 = T_C T_H T_{2L}$  are comprised of the constituent matrices

$$T_{2L} = \begin{bmatrix} 1 & 0 \\ \frac{1}{j\omega 2L} & 1 \end{bmatrix}, \quad (\text{A3})$$

$$T_H = \begin{bmatrix} \cos\left(\frac{\beta d}{2}\right) & jZ_o \sin\left(\frac{\beta d}{2}\right) \\ jY_o \sin\left(\frac{\beta d}{2}\right) & \cos\left(\frac{\beta d}{2}\right) \end{bmatrix} \quad (\text{A4})$$

and

$$T_C = \begin{bmatrix} 1 & \frac{1}{j\omega C} \\ 0 & 1 \end{bmatrix}. \quad (\text{A5})$$

## References

- [1] Kock W E 1948 Metallic delay lenses *Bell Syst. Tech. J.* **27** 58
- [2] Brown J and Jackson W 1955 The properties of artificial dielectrics at centimetre wavelengths *Proc. IEE B* **102** 11–6
- [3] Veselago V G 1968 The electrodynamics of substances with simultaneous negative values of  $\epsilon$  and  $\mu$  *Sov. Phys.—Usp.* **10** 509–14
- [4] Shelby R A, Smith D R and Schultz S 2001 Experimental verification of a negative index of refraction *Science* **292** 77–9
- [5] Iyer A K and Eleftheriades G V 2002 Negative refractive index metamaterials supporting 2-D waves *IEEE MTT-S International Microwave Symposium Digest (Seattle, WA 2–7 June 2002)* vol 2, pp 1067–70
- [6] Caloz C, Okabe H, Iwai H and Itoh T 2002 Transmission line approach of lefthanded materials *USNC/URSI National Radio Science Meeting Digest (San Antonio, TX 16–21 June 2002)* p 39
- [7] Sanada A, Caloz C and Itoh T 2004 Planar distributed structures with negative refractive index *IEEE Trans. Microwave Theory Tech.* **52** 1252–63

- [8] Eleftheriades G V, Iyer A K and Kremer P C 2002 Planar negative refractive index media using periodically L-C loaded transmission lines *IEEE Trans. Microwave Theory Tech.* **50** 2702–12
- [9] Grbic A and Eleftheriades G V 2003 Dispersion analysis of a microstrip based negative refractive index periodic structure *IEEE Microwave Wireless Components Lett.* **13** 155–7
- [10] Grbic A and Eleftheriades G V 2003 Periodic analysis of a 2-D negative refractive index transmission line structure *IEEE Trans. Antennas Propag. (Special Issue on Metamaterials)* **51** 2604–11
- [11] Grbic A and Eleftheriades G V 2004 Overcoming the diffraction limit with a planar left-handed transmission-line lens *Phys. Rev. Lett.* **92** 117403
- [12] Goussetis G, Feresidis A P, Wang S, Guo Y and Vardaxoglou J C 2005 Uniplanar left-handed artificial metamaterials *J. Opt. A: Pure Appl. Opt.* **7** S44–S50
- [13] Christopoulos C 1995 *The Transmission-Line Modeling Method: TLM* (Piscataway, NJ: IEEE Press)
- [14] Grbic A and Eleftheriades G V 2005 A 3-D negative-refractive-index transmission-line medium *IEEE AP-S/URSI International Symposium (Washington, DC, 3–8 July 2005)*